IET Image Processing

Review Article

IET Journals
The Institution of Engineering and Technology

Survey on mixed impulse and Gaussian denoising filters

ISSN 1751-9659
Received on 18th October 2018
Revised 2nd November 2020
Accepted on 1st December 2020
E-First on 23rd February 2021
doi: 10.1049/iet-ipr.2018.6335
www.ietdl.org

Mehdi Mafi[1] ✉, Walter Izquierdo[1], Mercedes Cabrerizo[1], Armando Barreto[1], Jean Andrian[1], Naphtali David Rishe[2], Malek Adjouadi[1]

[1]*Center for Advanced Technology and Education, Department of Electrical and Computer Engineering, Florida International University, Miami, FL, USA*

[2]*School of Computing and Information Sciences, Florida International University, Miami, FL, USA*

✉ *E-mail: mmafi002@fiu.edu*

Abstract: This study presents a comprehensive survey on mixed impulse and Gaussian denoising filters which are applied to an image in order to gauge the effects of this type of noise combination and to then determine optimal ways that can overcome such effects. The random noise model considered in this survey is the combined effect of impulse (salt and pepper) and Gaussian noise. After describing the noise models, the denoising filters which are applied to the images are classified and explained according to their design structure, the type of filters they use, the noise level they could overcome, and the limitations they face. This survey covers all related denoising methods and provides an assessment of the strengths and practical limitations of the different classes of denoising filters.

1 Introduction

Noise remains as a ubiquitous phenomenon that affects in different ways digital images. Generally, noise reduces the quality of an image, resulting in the loss of important details and degrading key features and textures. It can originate from many sources including image sensors, scanners, as well as other elements that relate image acquisition. Other sources include communication and transmission devices, atmospheric disturbances, relative motion, high resolution, and other unpredictable factors. Impulse noise and Gaussian noise are the two common types of image noise, which are considered in this survey. Impulse noise, also known as salt and pepper noise, appears as black pixels in white regions and white pixels in black regions. They are caused by A/D converter, transmission errors, memory location, and faulty pixels in camera sensors [1, 2]. The noise model is assumed as [3–5]

$$I(c) = \begin{cases} c_{\min} & \text{Probability } P_s \\ c_{\max} & \text{Probability } P_p \\ c_{\min} < c < c_{\max} & \text{Probability } 1 - P_p - P_s \end{cases} \quad (1)$$

In (1), $c_{\min}$ and $c_{\max}$ are the minimum and maximum values which are 0 and 255 in the 8-bit resolution images [6].

Gaussian noise is another type of noise which is additive and independent. It can be the product of sources such as amplifiers, shot noise [6], film grain noise [2], among others. The noisy image is as expressed in

$$I_n(i, j) = I(i, j) + n(i, j) \quad (2)$$

where I_n is the noisy image, I is the original image and n defines the additive noise. One of the main effect of Gaussian noise is the blurring of image details, with a pronounced effect especially on the edges. The noise assumes a Gaussian distribution [2, 7, 8]. A comprehensive survey on impulse and Gaussian denoising filters is provided in [9]. In this initial phase of this survey, the focus is placed more on their effect on the image when they happen in isolation. However, as this survey intends to show, the challenge of denoising an image becomes even more complicated when these two sources of noise are mixed. Therefore, the denoising filters are implemented based on the nature of the mixed noise which is a combination of additive and non-additive noise. A block diagram showing the different classes of denoising filters is as shown in Fig. 1.

2 Denoising filters

2.1 Spatial filters

Spatial filters, as their name indicates, are defined in the spatial domain in which the intensity of each pixel is changed based on the intensities of its neighbourhood pixels.

2.1.1 Non-linear filters: A non-linear filter is a type of filter in which its output is a non-linear function of its input.

Non-local mean (NLM)-based filters: The NLM filters are based on the weighted mean value of all pixels in the image as well as how similar they are to the pixel being processed. A combination of NLM filter [10, 11] and trilateral filter [12], which is an extension of bilateral filter [13], is used in a patch-based weighted mean filter (PWMF) [14] and mixed noise filter (MNF) [15].

The PWMF method is based on the convergence theorem in the distribution for NLM [16] in order to show the rate of convergence of the NLM filter in the presence of Gaussian noise. Convergence distribution has two definitions; similarity and dependency. In its similarity definition, the patches $v(N_i)$ and $v(N_j)$ in the $D \times D$ predefined window ($N_i(D)$) are similar when they have the same probability distribution. In l-dependent definition, if the distance of random variables which correspond to the patches centred at (i) is greater than an integer $l \geq 0$, then the random variables are independent. The trilateral filter [12], first detects the impulse noise based on the statistic rank of ordered absolute differences (ROADs), which is computed using the smallest Euclidean distance within the predefined window ($N_i(D)$) with centre i and size $D \times D$, and if it is large, the pixel being processed is considered impulse noise. Afterwards, it uses ROAD statistic to define the final weight.

Both PWMF and MNF methods are defined as in (3); this is the same definition used for NLM and trilateral filters.

$$\hat{v}_i = \frac{\sum_{j \in N_i(D)} w(i,j) v_j}{\sum_{j \in N_i(D)} w(i,j)} \tag{3}$$

where $\hat{v}_i$ is the denoised pixel, v_j is the grey value in a window $N_i(D)$, and $w(i, j)$ is the final weight. The final weight is different in PWMF and MNF methods. In PWMF, the final weight is a multiplication of three exponential weights obtained from the combination of NLM, consisting of two weights based on Euclidean distance and l-norm, and one weight based on ROAD statistics. In MNF, the final weight is a multiplication of two exponential weights obtained from the combination of NLM which contains a weight based on Euclidean distance and l-norm, and another weight based on ROAD statistics. The PWMF method is known to produce better results than the method in [17], ROLD-EPR [18] which is a variant of ROAD statistics, and trilateral filter [12]. MNF method on the other hand produces better results than the trilateral filter [12].

The optimal weight mixed filter in [19] is based on the optimal weights of NLM filter [20] and the filter in [21] with an improvement ROAD statistic [12]. The proposed ROAD with a mixture of Gaussian and impulse noises (ROADGI) as given in (4) is shown to be more stable

$$\mathrm{ROADGI}(x_0) = \left(\frac{1}{k} \sum_{i=1}^{k} r_i(x_0) - \sigma \right) \tag{4}$$

where $r_i(x_0)$ is the ith smallest term in distance between data patches, k is between 2 and the cardinality of set $\Omega^0_{x_0,d}$, $\Omega^0_{x_0,d}$ is defined as $\{x : 0 < N \| x - x_0 \|_\infty \leq d\}$, d is a positive integer, x represents the pixels in the image and σ is the Gaussian noise level. This could work in combination with weights optimisation and joint impulsivity [12, 15]. Finally, the denoising filter can be obtained based on modifications of the trilateral filter [12]. This process is shown to lead to better performance than the trilateral filter [12], the PARIGI method [22] and the filter with patch-based weighted means [23].

Bilateral based filters: The robust local similarity filter in [24] is based on the weighted averaging filter (i.e. bilateral filter) with a new similarity measure among blocks. It uses the sum of distances between a given pixel and the most similar pixels in the selected window, which means similarity between a pixel under process and its neighbouring pixels is measured instead of performing a comparison of pixels directly. The proposed filter is defined in (5)

$$y = \frac{\sum_{j=1}^{N} w_j x_j}{\sum_{J=1}^{N} w_j}, \quad w_j = \mathcal{K}\left(\frac{1}{\alpha} \sum_{k=1}^{\alpha} d_{j(k)} \right) \tag{5}$$

where y is the output, N is the number of pixels in the image, w_j is weight, $d_{j(k)}$ is the smallest Euclidean distance between x_j and the pixels in the selected window, $\mathcal{K}$ is the kernel function (e.g. Gaussian). The results obtained in [24] show a better performance than the fuzzy vector median filter and the fuzzy vector directional filter in [25], the fuzzy ordered vector median filter and the fuzzy ordered vector directional filter in [26], the adaptive nearest-neighbour filter in [27], the adaptive nearest-neighbour multichannel filter in [28], the directional distance filter in [29], the alpha-trimmed vector median filter in [30], the hybrid directional filter (HDF), the entropy vector median filter and the adaptive HDF described in [31].

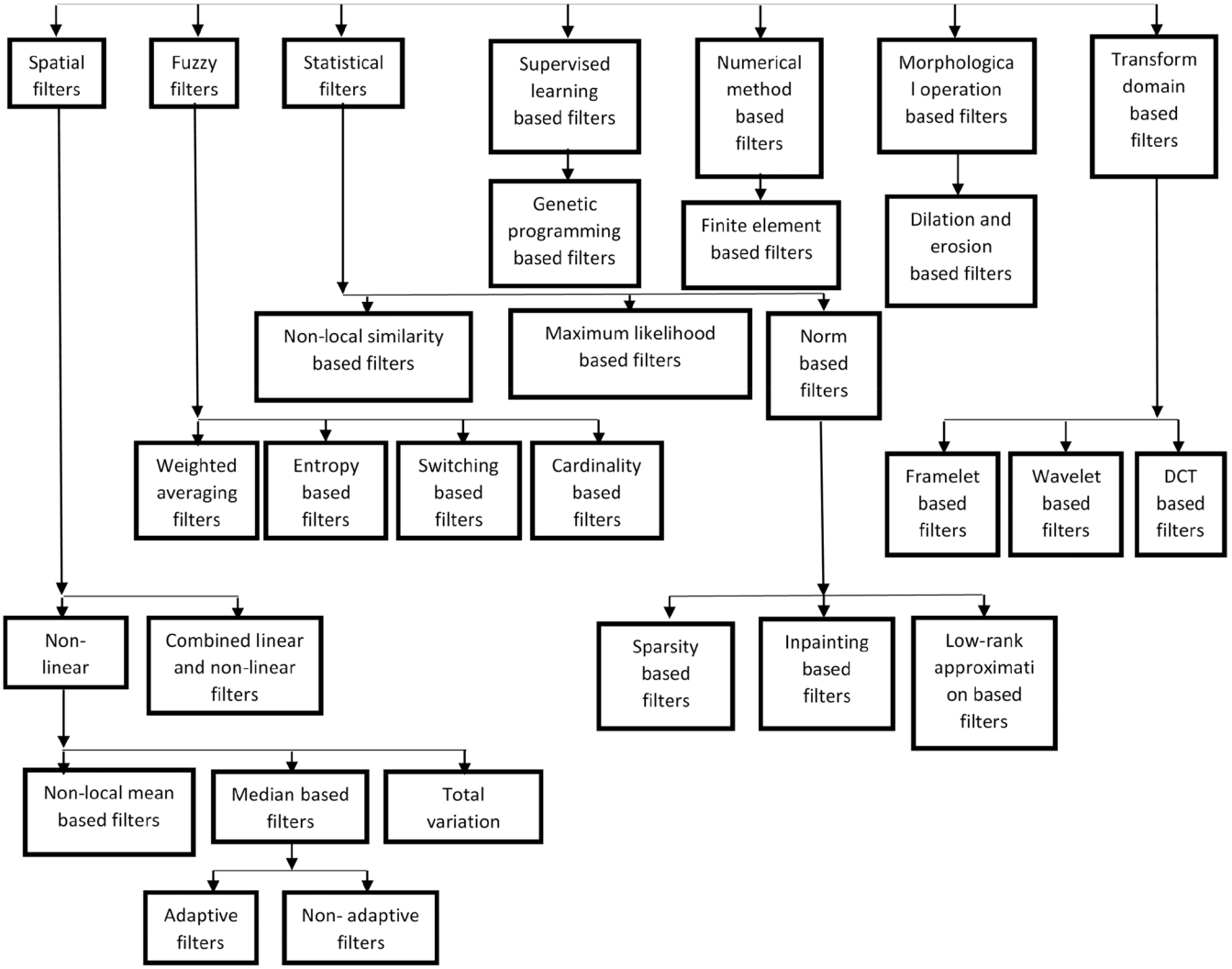

Fig. 1 *Block diagram of the different classes of denoising filters*

In the proposed work median-based filters of the following types are studied:

Non-adaptive median-based filters: The proposed filter in [32] is a non-linear filter, and its implementation consists of the following steps: (i) segment the image into different regions, (ii) determine the Gaussian distribution, (iii) calculate the median value of the pixels, (iv) remove the corrupted pixels, (v) reconstruct the denoised image sections, and (vi) obtain the final denoised image. This proposed filter was successfully applied to computed tomography scans with low image quality.

Adaptive median-based filters: Adaptive median filters (AMFs) in general yield good performance in eliminating impulse noise [33, 34], and averaging filters yield good performance in eliminating Gaussian noise instead. Their combination can thus be very effective in eliminating these noises when mixed. An adaptive weighted mask [35] is used to remove mixed noises based on the median filter. The median filter which is good for salt and pepper noise replaces the minimum or maximum values of the predefined window. The size of the mask is defined according to some number of minimum and maximum values. The weighted averaging is defined for each pixel as (6) considering an $N \times N$ image $f(x, y)$

$$g(i, j) = \sum w_{f(x,y)} \times f(x, y) \tag{6}$$

where $w_{f(x,y)}$ is the similarity-based weight as $w_{f(x,y)} = \left(\text{similarity}_{f(x,y)} / \sum \text{similarity}_{f(x,y)}\right)$, $\text{similarity}_{f(x,y)} = e^{(1/|f(x,y)-\mu|/\sigma(i,j))}$, and where μ is the mean and σ is the standard deviation of the predefined window. According to [18], the adaptive weighted mask produced better results than the median and average filters.

Total variation filters: Total variation method assumes that the total variation and consequently the integral of the gradient of the signal are high. Therefore, by decreasing the total variation, a denoised image with high similarity is obtained. The method proposed in [36] is based on the total variation [37] which has two steps: noise detection and total variation minimisation [38]. First, AMF [39] and adaptive centre-weighted median filters (ACWMFs) [40–42] are used. Afterwards, the deblurring is applied to the image in the noise-free pixel locations by minimising the objective function and also, solving a linear equation. Then, total variation regularisation is applied to the image in order to smooth the noise and remove the noisy pixels.

Another total variation-based method [43] detects the corrupted impulse noise with AMF [39] (salt and pepper) or with the centre-weighted median filter [44] (a random value impulse noise). Then, a cost function which is a combination of total variation regularisation [45] and l_1 and l_2 norms are applied to the image in order to remove Gaussian and impulse noises, respectively. Finally, the denoised image is obtained by using the iteratively reweighted norm algorithm [46, 47] and by replacing the l_1 norm by a weighted l_2 norm.

The filter described in [48] is a combination of L^1L^2 data fidelity and total variation regularisation [49]. This minimisation is based on the locally varying regularisation. Consequently, a spatially local parameter is automatically selected based on locally adapted algorithms [50] and primal-dual algorithm for locally adaptive total variation [51]. The minimisation problem is as defined below

$$\min_{u \in BV(\Omega)} \alpha_1 \| T_1 u - g_1 \|_{L^1(\Omega)} + \alpha_2 \| T_2 u - g_2 \|^2_{L^2(\Omega)} + \int_{\Omega} \lambda(x) |Du| \tag{7}$$

where u is the image, Ω is an open bounded domain (Lipschitz boundary), $T_i : L^i(\Omega)$ is a bounded linear operator, g_i is a datum, $\alpha_i \geq 0$ and α_1 is large in the presence of dominant impulse noise and α_2 is large in the presence of Gaussian noise, λ is a function and is selected automatically in this particular study, and $\int_{\Omega} |Du|$ defines the total variation.

2.1.2 Combined linear and non-linear filters: The non-linear median filter has good performance in removing impulse noise. If the median filter is combined with a linear filter, the combination is seen to be effective in removing the mixed impulse and Gaussian noise. The filter in [52], uses a combination of median filter [53, 54], Wiener filter [53, 54], and bilateral filter [13] in order to remove mixed noises. The authors of [52] claimed that wavelet techniques produce blur image, therefore, this combination (median filter, Wiener filter, and bilateral filter) produces a good quality image with more details.

2.2 Fuzzy filters

2.2.1 Weighted averaging filters: The weighted averaging filters are based on weights, where the centre value is often given more weight. They apply weights to the pixels being processed by using a sort of averaging in which the summation of them is used as the denominator. The weights can be obtained in different ways one of them is based on fuzzy logic. There are some methods which are based on fuzzy weights [55, 56]. They use fuzzy peer group of the central pixel in the selected window [57] in a two-steps approach: (i) impulse detection (ii) Gaussian smoothing. The first step involves checking the certainty of the two fuzzy rules: (i) best number of members determination (m) for peer groups [58] associated with the central pixel (x_m) and (ii) accumulated similarity which is a summation of values of membership function (ρ) for all neighbouring pixels around the central pixel. If the accumulated similarity is large and if the mth member is similar to the central pixel in the selected window, then the certainty of the second rule is computed. This certainty is equal to a multiplication of these two values by using a t-norm product and is compared to a predefined threshold $\in [0, 1]$. If it is equal or greater than the threshold, the pixel being processed is assumed noise free, otherwise, it is an impulse noise and the vector median filter (VMF) method [59] is applied in order to remove it. The second step involves, the fuzzy averaging among a fuzzy peer group of the pixel being processed and is applied as below

$$F_{\text{out}} = \frac{\sum_{i=0}^{\hat{m}} \rho(x(i)) x(i)}{\sum_{i=0}^{\hat{m}} \rho(x(i))} \tag{8}$$

Another fuzzy weight-based filter [60] defines three fuzzy sets (small, medium, and large) containing triangular membership functions. Small weights are assumed for noisy pixels and larger weights are considered for noise-free pixels. Finally, the centre of gravity (COG) defuzzification [61, 62] is used in order to obtain the weights. The denoised image is obtained based on a weighted averaging filter as

$$\hat{x}_i = \sum_{i=0}^{m^2} w_i x_i / \sum_{i=0}^{m^2} w_i \tag{9}$$

where $\hat{x}_i$ is the estimated denoised pixel, w_i is the associated fuzzy weight, and x_i ($i = 1, 2, \ldots, m^2$) are the pixels in the $m \times m$ selected window.

2.2.2 Entropy-based filters: The concept of entropy refers to a statistical measure of randomness that is helpful in analysing the texture of the image. Some filters use this concept in order to perform image restoration. The method proposed in [63] is based on the fuzzy entropy concept. It consists of three phases: (i) definition of the information sources based on region fuzzy entropy as well as directional structure features, (ii) triangle module fusion operator implementation, and (iii) application of a hybrid filter. It compares the triangle module operator [64] as defined in (10) with a predefined threshold. If it is less than the threshold, the hybrid filtering method – AMAWM [65] is applied for denoising, otherwise, the pixel is left unchanged

$$F_{i,j}(R, D) = \frac{RD}{1 - R - D + 2RD} \tag{10}$$

where R and D are the region's fuzzy entropy with 3×3 window and direction gradient in the different directions. Fuzzy entropy is based on the concept of entropy in which its variable is defined as a membership function [66] [67]. Direction gradient is equal to a maximum of the fuzzy entropy in different directions and assumes the pixel being processed with the large gradient as an edge point.

2.2.3 Switching-based filters: Some filters in the noise detection phase are based on the switching process in order to select the optimal output. The method in [68] uses both fuzzy switching filter and the bilateral filter to remove the impulse and Gaussian noise, respectively. It generates four input images (by rotating at multiples of 90°) and then applies fuzzy sigma VMF (SVMF) [69] in order to restore them. SVMF consists of two steps: (i) noise detection and (ii) SVMF. In the noise detection step, the aim is to determine the membership function degree of each pixel. Therefore, in the first rule, the mean difference of neighbourhood around the central pixel (x_i) in the selected window is computed; if it is large, the pixel being processed is assumed noisy. In the second and third rules, the basic gradient of each eight neighbours for each pixel is computed. In the second rule, if the basic gradient is not large and the two related gradients (gradients in the same direction) are large or vice versa, then pixel being processed in that direction is assumed as part of the impulse noise. In the third rule, if the basic gradient is large and the two related gradients are large or vice versa, then the pixel in that direction is not part of the impulse noise and should be kept as is. In the fourth rule, the membership degree of each pixel in the fuzzy noise-free set is checked, and if each colour pixel component is not noisy, then the colour pixel being processed is assumed to be part of the impulse noise. In the SVMF step, if the aggregated distance (L) is greater than the threshold (T), the output of SVMF is replaced by the vector median ($\boldsymbol{x}_{(1)}$), otherwise, it is left unchanged. L and T are defined as

$$L = \sum_{i=1}^{N} \| \boldsymbol{x}_{(1)} - x_i \| \quad \text{and} \quad T = L + \frac{\lambda \times L}{N-1} \tag{11}$$

where λ is a constant to be selected within a specified range and N is the window size. Then, the four SVMF outputs are restored and the output image is obtained by the median vector of these four restored SVMF (median of colour samples from the same spatial position in the restored images). Finally, a bilateral filter [13] is applied in order to remove Gaussian noise. The results [68] show a better performance than VMF [59] and bilateral filter [13].

2.2.4 Cardinality-based filters: Cardinality is defined as number of elements in a set. The method in [70] which is an improvement on simple fuzzy rule (SFR) [71] and VMF method [59] uses the Cardinality concept. First, it detects the impulse noise by detecting the 0's and 255's pixels in the scanning window. In order to calculate similarity variable, three fuzzy rules which are based on a membership function with high, medium and low sets are defined, then the COG defuzzification [61, 62] is used in order to get weights (w_k). The weights are improved in such a way in which if the pixel is impulse noise, then, the final weights are computed, otherwise, they are left unchanged. Then, by setting a threshold (0.8 proposed in [70]), a set of final weights which are greater than predefined threshold is selected (G). Therefore, in order to eliminate denoised pixel, the cardinality (C) of G is used. If C is >1, the alpha trimmed mean technique is applied to the noisy pixel as shown in (12), otherwise, the convex hull technique is applied [72] to the noisy pixel instead.

$$\text{Alpha trimmed} = \frac{1}{C-y} \sum_{r=y+1}^{C-k} G, \quad \text{and} \quad y = C \times \frac{0.35}{2} \tag{12}$$

with k being the number of weights used. Results given in [70] show that alpha trimmed mean technique produced better performance than VMF [59] and SFR [71].

2.3 Statistical filters

These types of filters are based on key statistical parameters. This survey divides them into the following categories: (i) norm-based filters, (ii) Non-local similarity-based filters, and (iii) maximum likelihood estimation (MLE)-based filters. Details on these categories are described in the following sections.

2.3.1 Norm-based filters: Norm is a statistical average and can be defined as a function in which the size or length of each vector (in a vector space) is set to be positive.

Sparsity-based filters: Sparse approximation can be defined as a sparse vector in which a system of equations is solved. By adding some information while preventing overfitting, sparse regularisation is obtained. Both sparsity and sparse regularisation select the best input variables (reduced input variables) in order to learn about the output variables. A sparsity-based algorithm in [73] proposed a $l_1 - l_0$ minimisation in which l_0 is used for impulse detection and l_1 is used for sparse representations over an unknown dictionary. Based on the approach considered in [74], the method presented in [73] has three phases: (i) impulse detection based on AMF [39] and ACWMF [40–42] methods, (ii) restoration of the image from an unknown dictionary by using proposed modified K-SVD (MK-SVD) [73, 75] with image reconstruction by averaging the patches and noisy image, and (iii) implementation of an additional l_1 norm in order to carry out a false detection and alternating $l_1 - l_0$ minimisation. The K-SVD is a dictionary learning algorithm via a singular value detection and it is a generalisation form of the k-means clustering algorithm. MK-SVD does not have a good performance in the presence of high impulse noise, therefore, step three is applied in order to improve the denoising results. From the results obtained, this three-step method outperformed AMF [39], ACWMF [40–42], MK-SVD, the two-phase deblurring/denoising (TPD), and other methods introduced by Cai *et al.* [74, [76], Wang and Wu [77], and Nikolova [78].

The method in [79] is based on an approach which uses the sparse representation of patches in a dictionary. Also, l_0-quasi and l_1 are responsible for sparse representation and sparsity of residual, respectively. The method has also three steps: (i) dictionary learning, (ii) impulse detection, and (iii) iterative minimisation algorithm. In the first step, the offline dictionary is learned by independent component analysis, claiming better results than 1-based dictionary learning [80]. In the second step, the ROAD [12] algorithm is used for impulse detection. In the third step and for every patch, a non-convex minimisation problem as (13) is solved iteratively by a combination of soft [81] and hard thresholding [82].

$$\min_{x,f} \frac{1}{2} \| \Omega \otimes (y - \boldsymbol{x}\Phi - \boldsymbol{f}) \|_2^2 + \lambda_1 \| \boldsymbol{x} \|_1 \quad \text{subject to} \| \boldsymbol{x} \|_1 \leq \lambda_2 \tag{13}$$

where y is the noisy image, Ω is the location of pixels which are not affected by impulse noise, Φ is the learned dictionary, $\boldsymbol{x}$ is the vector of coefficients, $\otimes$ is the component-wise multiplication, $\boldsymbol{f}$ is the sparse vector of pixels which are affected by impulse noise, λ_2 and λ_2 are regularisation parameters. It claims to have better results than the method in [73] and the method in [17].

The weighted encoding with sparse non-local regularisation (WESNR) is proposed in [83]. It does not have the impulse noise detection step because of generating artifacts in high noise levels. The image can be defined as

$$x = \boldsymbol{\alpha}\Phi \tag{14}$$

where x is the original image, Φ is the dictionary and $\boldsymbol{\alpha}$ is a coding vector. In order to denoise the image, optimal estimation of $\boldsymbol{\alpha}$ should be calculated by encoding the noisy image (y) over the dictionary. Owing to the two different noise categories, the weight (close to 1 for pixels corrupted by Gaussian noise and smaller weights (w) for pixels corrupted by impulse noise) is assigned to residuals ($y - \boldsymbol{\alpha}\Phi$), therefore, an optimal estimation for $\boldsymbol{\alpha}$ is

defined in the presence of mixed noise as (15) which is based on sparse regularisation

$$\hat{a} = \arg\min_{\alpha} \| W^{1/2}(y - \boldsymbol{\alpha}\Phi) \|_2^2 + \lambda R(\boldsymbol{\alpha}) \quad (15)$$

where λ is the regularisation parameter, $R(\boldsymbol{\alpha})$ is the regularisation term given as $\lambda\| \boldsymbol{\alpha} - \boldsymbol{\mu} \|_1$ and $\boldsymbol{\mu}$ is the non-local coding vector. The regularisation term is obtained by integrating sparsing and non-local self-similarity (NLSM) together. This integration can improve WESNR. In order to learn a set of PCA dictionaries of natural images, the paper [83] used the proposed algorithm in [84]. It claims that has better result than ROR-NLM [85], Cai *et al*. [74], $l_1 - l_0$ [73], TF [12] and M + BM3D [86].

In-painting-based filters: Image in-painting occurs when there are damaged image pixels and missing image pixels. The image is reconstructed from background information. The proposed method in [87] is based on two algorithms: (i) in-painting using l_0 minimisation (ii) inpainting adaptive outlier pursuit (AOP). Also, in order to detect the impulse noise, it [87] uses AMF [39] and ACWMF [40–42]. The difference between two algorithms is related to l_0 term, which in first algorithm is put in objective function and in the second algorithm l_0 is constraint. Also, the AOP can find the sign flips (outliers) and reconstruct the data by using the other correct measurements. The performances of both methods are similar. Finally restored image is obtained by iteratively solving the minimisation problem for both algorithms.

Low-rank approximation-based filters: Low-rank approximation is a minimisation problem and it is based on Frobenius norm in which the cost function calculates the fit between a given data and an approximating optimisation variable, subject to a constraint that the approximating the optimisation variable has reduced rank. The method in [88] is based on low-rank approximation and uses the weighted low-rank model as weighted low-rank approximation (WLRA) [89, 90] or representation (WLRR) [91, 92]. The proposed WLRA and WLRR which are based on LRA [90] and LRR models are shown in (16) and (17), respectively.

$$\min_{\boldsymbol{XD}} \frac{\lambda}{2}\| W \odot (\boldsymbol{Y} - \boldsymbol{X})| \|_{\mathrm{F}}^2 + \frac{\beta}{2}\| \boldsymbol{X} - \boldsymbol{D}) \|_{\mathrm{F}}^2 + \| \boldsymbol{D} \|_* \quad (16)$$

$$\min_{\boldsymbol{XZ}} \frac{\lambda}{2}\| W \odot (\boldsymbol{Y} - \boldsymbol{X}) \|_{\mathrm{F}}^2 + \frac{\beta}{2}\| \boldsymbol{X} - \boldsymbol{XZ}) \|_{\mathrm{F}}^2 + \| \boldsymbol{Z} \|_* \quad (17)$$

where $\boldsymbol{X}$ is a low-rank matrix and noiseless counterpart of $\boldsymbol{Y}$, also, $\boldsymbol{Y}$ is a matrix which its columns are a sort of vectorised patches, $\boldsymbol{D}$ and $\boldsymbol{Z}$ are low-rank matrices, $\| \boldsymbol{D} \|_*$ is nuclear of $\boldsymbol{D}$, $\| \boldsymbol{Z} \|_*$ is nuclear of $\boldsymbol{Z}$, $\odot$ is the element-wise product and $\beta, \lambda > 0$ are constants, W is exponential assigned weight to residual approximation $(\boldsymbol{Y} - \boldsymbol{X})$ and $\| \ . \ \|_{\mathrm{F}}$ is the Frobenius norm.

WLRA and WLRR show a good performance in removing the impulse noise by choosing appropriate weights. For corrupted pixels, the weights are small, but, for uncorrupted pixels, the weights are close to 1. Then, the aforementioned equations are solved by alternatively solving for $\boldsymbol{X}$, W and D(or Z). Finally, the noisy image is reconstructed by putting non-local similar patches to a matrix as well as finding WLRA or WLRR. It claims that has better performance than AMF [39], median and AMF coupled with spatially adaptive iterative singular- thresholding algorithm [93], median filter coupled with median coupled with BM3D (M/AMF-BM3D) [94], AMF coupled with BM3D (AMF-BM3D) [95], ROR-NLM [85], median and AMF coupled with LRR/LRA (M/AMF-LRA/LRR).

Another low-rank approximation-based algorithm is defined in [96]. It is based on Laplacian scale mixture (LSM) modelling and non-local low-rank regularisation. Impulse noise is modelled with LSM distribution and after noise estimation, a non-local low-rank approximation is used for denoising process. Non-local low-rank is based on NLSM and low-rank approximation of the image. In order to model the impulse noise with LSM, the maximum a posteriori (MAP) estimator is defined in (18) to estimate the x, s, and, σ values.

$$\begin{aligned}(x, s, \theta, \sigma_w) = \arg\min \frac{1}{2\sigma_w^2}\| y - x - s \|_2^2 \\ +\sqrt{2}\sum_i \frac{|s_i|}{\theta_i} + 2\sum_i \log\theta_i + \eta J(x) + N\log\sigma_w\end{aligned} \quad (18)$$

where θ is the standard deviation, Λ is diag (α_i), y is the observed noisy image, x is the original image, α_i is the random variable, which has a Laplacian distribution, σ_w is the variance of AWGN, η is the free parameter, N is the number of pixels, ε is the small constant, w_i is the AWGN at position i, $s_i = y_i - x - w_i$ is the outlier component caused by impulse noise and $J(x)$ is the energy of the configuration of x. For non-local rank regularisation, a combination of LSM model in (17) and low-rank regularisation model in [97] is used with the assumption that each similar patch is dependent. Then, the proposed objective function will be as expressed as (see (19)) . Also, In order to use a smooth surrogate of rank (.), $\eta\sum^{\mathrm{rank}}(\tilde{\boldsymbol{R}}_j\boldsymbol{x})$ is replaced by $\eta\sum_j L(\tilde{R}_j x, \varepsilon)$. Where $\tilde{\boldsymbol{R}}_j\boldsymbol{x}$ is a matrix formed by the set of similar patches, $L(\boldsymbol{x}, \varepsilon) = \sum_{r=1}^{r_0}\log(\sigma(\boldsymbol{x}) + \varepsilon)$, $\boldsymbol{x}$ is a matrix with size $(n \times m)$, $\sigma_r(\boldsymbol{x})$ is the rth singular value of $\boldsymbol{x}$, r_0 is min (n, m).

Finally, the denoising is improved by exploiting group sparsity of similar patches. Finally, (17) is solved by using the optimisation algorithm for θ, α, x, and σ_w. Empirical results show that the LSM method outperformed the TPD method or Cai *et al.* [76], the sparse and low-rank regularisation (SLR) denoising method [98], the WESNR method [83], the well-known BM3D [95], non-locally centralised sparse representation method [99] and l_p-norm (instead of LSM) with NLR (l_0/l_1-NLR).

2.3.2 Non-local similarity-based filters: In non-local similarity-based filters, several similar patches are used to reconstruct the under-processed patch. A non-local similarity filter is introduced in [100] which has several steps. First, it proposes the use of a statistical adaptive curvelet thresholding criterion in order to characterise the disruptions that appeared during the denoising process. Second, it uses a new statistical technique (De-JASP) based on joint adaptive statistical prior (JASP), which is a combination of local smoothness and geometry regularity of an image. This combination is obtained by using the discrete curvelet transform [101] and NLSM prior in the three-dimensional (3D) transform domain [102] with a regularisation parameter (it is multiplied to NLSM term) in order to control for the tradeoff between the two-terms. Then, a regularisation-based framework is considered by putting the proposed variational JASP (De-JASP) as $y(x)$ to the minimisation process defined in

$$\min_u \frac{1}{2}\| \boldsymbol{\varphi} \bigcirc (y - x)| \|_{l_2}^2 + \lambda\mathscr{Y}(x) \quad (20)$$

where y is the noisy image, x is the clean image, λ is the regularisation term, $\bigcirc$ is an element-wise multiplication, $\boldsymbol{\varphi}$ is a degradation matrix. Finally, the alternating minimisation problem in (17) is solved by using the split Bregman iterative algorithm [103]. This method has yielded better results than the iterative framelet-based approximation/sparsity deblurring algorithm

$$\begin{aligned}(x, \alpha, \theta, \sigma_w) = \arg\min \frac{1}{2\sigma_w^2}\| y - x - \Lambda\theta \|_2^2 \\ +\sqrt{2}\sum_i |a_i| + 2\sum_i \log(\theta_i + \varepsilon) + \eta\sum_j \mathrm{rank}(\tilde{\boldsymbol{R}}_j\boldsymbol{x}) + N\log\sigma_w\end{aligned} \quad (19)$$

IFASDA [104], and image denoising via joint statistical modelling [103].

2.3.3 MLE-based filters: MLE is based on a statistical model and it is a special case of MAP estimation. In order to perform parameter estimation, MLE finds the values that maximise the likelihood of them. The PARIGI method in [22] is based on a patch-based approach and has two steps: in the first step, impulse noise is estimated by using ROADs [12] in which summation of four smallest distances are calculated from the pixel being processed in the selected window. Then, the summation is compared with a threshold (70 is proposed in [22]), if it is greater than the threshold, the under-processed pixel is noisy. In the second step, the estimator at each point is computed, therefore, a corresponding subset (ρ) of the n-nearest neighbours of square image patch defined in the patch domain for distance (D_w) is calculated. D_w is based on the binomial distribution probability as defined below

$$D_w(P,Q) = \sum_{k=1}^{(2N+1)^2} w_k |P-Q|_{(k)}^2 \tag{21}$$

$$w_k = B\left((2N+1)^2, k, (1-p)^2\right) \tag{22}$$

where w_k are weights, $|P-Q|$ is the distance between two patches, p is the impulse noise, $(2N+1)^2$ is the patch size, k is the parameter of the binomial distribution ($0 \le k \le n$) and n is the number of weights. Maximum likelihood estimator MLE $(\hat{u}(x), \hat{\sigma}(x))$ is computed at each point based on values in the corresponding subset (ρ) centred at x. Finally, in order to remove the remaining impulse noise, another estimated image $u_2(x)$ is obtained using (23) and (24) and the denoising process is repeated for $u_2(x)$ to obtain the denoised image $\hat{u}_2(x)$. This process may be repeated as needed.

$$u_2(x) = \hat{u}(x).1_{x \in M} + u(x).(1 - 1_{x \in M}) \tag{23}$$

$$M = \left\{x \in \Omega; \left|\hat{u}(x) - u(x)\right| > \hat{\sigma}(x)\right\} \tag{24}$$

where Ω is the image domain, $\hat{u}(x)$ is the denoised image, $u(x)$ is the clean image, and $\hat{\sigma}(x)$ is the estimated variance.

2.4 Supervised learning algorithm-based filters

Supervised learning is a machine learning task in which the output is known for the network on the basis of a labelled training set [105]. It iteratively makes predictions on the training data. The method in [106] is based on a switching scheme with two noise detectors and two estimators for noise removal. Most of the noise is captured with the first detector and the remaining noise hidden in the image details or close to the edges is detected by a second detector. Each detector has its own estimator based on median and median absolute deviation (MAD). Also, in order to build detectors, genetic programming (GP) is used [107, 108]. It requires some steps including representation, initialisation, selection, terminal set, function set, and training set to build the detectors. In training sets, the first detector is trained on a data set with a similar distribution of a typical noisy image. Although most of the noise is identified by the first detector, to identify the remaining noise, the data goes through a second detector. In the second detector, the data from the first detector are filtered and only the noise-free samples are selected in the trained detector and checked whether they are out of GP classification or not. If the pixel is out of GP classification, it is noisy, otherwise, it is noise-free. Finally, the first estimator defines the noisy pixel as

$$\varphi^{(1)}(x_{ij}) = \frac{1}{K^2 - 2[\alpha K^2]} \sum_{j=\alpha K^2+1}^{K^2-[\alpha K^2]} x_{(j)} \tag{25}$$

where x is the input image, $x_{(j)}$ is the jth order of elements of filtering window ($W_K(i,j)$), α is the trimmed mean, and K is the window size. The second estimator is as shown in (26). It is based on centre-weighted median (CWM) [44] and is appropriate for leaving the filtered pixel unchanged in the case of false detection

$$\varphi^{(2)}(x_{ij}) = \mathrm{CWM}_w(x_{ij}) = \mathrm{med}(W_k(i,j) \diamond w) \tag{26}$$

where $\diamond$ is w repetitions of the central pixel from the window ($W_K(i,j)$).

2.5 Numerical method-based filters

Finite element method (FEM) is a numerical approach used to solve the problem in which a vibrational formulation, post-processing and one or more solution algorithms are used. The method in [109] is based on FEM [110–112] and consists of three steps: (i) decomposition of the domain (Ω) into triangles or quadrilaterals, (ii) defining local basis functions in each triangle or quadrilaterals, and (iii) combine the local basis functions in order to form a set of global basis functions which span the finite element space. In the presence of only impulse noise, the scattered data interpolation (finite element interpolation [110, 112, 113]) based on Delaunay triangulation [114] (decomposition into triangles) or Voronoi cell (decomposition into polygons) [115, 116] can detect and remove noisy pixels. Interpolation phase finds the image function over piecewise polynomial interpolant. In the case of mixed impulse and Gaussian noise, it is necessary to smoothen the image. Therefore, the finite element smoothing is applied by minimising the functional equation involving the gradient of a finite element function as shown in (27). This is equivalent to the abstract vibrational problem over the finite element space function (V).

$$\min_{u \in v} \sum_{i=1}^{N} \left(u(x_i, y_j) - z_i\right)^2 + \lambda \int \| \nabla u \|^2 \mathrm{d}x\mathrm{d}y \tag{27}$$

where u is the piecewise polynomial space which is finite element space, z_i is the function given on a set of scattered points $(\{(x_i, y_i)\}_{i=0}^{N})$, λ is the positive constant and $V = \left\{u \in C^0(\Omega) \middle| u_{|T} \in p(T),\ T \in \mathrm{T}\right\}$, Ω is the convex hull of the set of scattered points, T is the structured decomposition of the rectangular domain Ω into rectangles or triangles, $p(T)$ is the linear or bilinear polynomial space on T (triangle or rectangular), $C^0(\Omega)$ is the space of a continuous function on Ω.

2.6 Morphological operation-based filters

These are non-linear operations based on the morphology of features in an image not necessarily related to numerical values. Dilation and erosion are two such morphological operators. Dilation adds pixels to the boundaries in the image and erosion removes the pixels on the boundaries. The method in [117] is based on the morphological operation. It proposes several toggle mappings with different criteria which are applied in order to detect the noise. The criteria for noise detection is contrast probability at the pixel under consideration. Contrast probability is defined as local contrast (absolute value of the difference between eight neighbouring pixels and mean value of these neighbouring pixels) over a summation of eight neighbouring pixels in the 3×3 selected window (or $\mu = 1$ size). In the selected window, if contrast probability at the pixel point is greater than critical probability which is defined according to window size (or different μ size) as $((1/(2\mu+1)(2\mu+1)) - 1)$ [118], then, the pixel being processed is considered noise. In order to eliminate the noise, toggle mappings are defined. They select the central pixel in which the noisy central pixel is replaced with morphological erosion and corrosion based on the image contrast.

The first proposed toggle mapping is based on the opening and closing operations. It can improve the contrast without any extra contours, but, it has a disadvantage in that it eliminates

unconnected narrow regions in which the structuring element does not fit. The noise criterion is contrast probability checking at the pixel point, if it is less than the critical probability, the pixel is left unchanged, otherwise, it is replaced with a multiplication of opening and closing operation.

The second proposed toggle mapping is based on white top-hat [118] (the difference between the original and the morphological opening image) and allows detection of noise only in white components and does not use a contrast measure nor a probability criterion. The noise criterion is top-hat checking at the pixel point; if it is equal or less than mean white top-hat, it is left unchanged, otherwise, it replaces with a multiplication of opening and closing operation. Then, the inverted image is cleaned in order to remove the noise.

The third toggle mapping is based on white top-hat. The noise criterion is top-hat checking at pixel point; if it is equal or less than mean white top-hat, it is noise, otherwise, it is replaced with a rank filter [119]. A rank filter ($(\rho_{\mu,k})$, $\mu = 1$, $1 \le k \le 9$, k is the number of applied filter) is obtained when the pixel in the structuring element is sorted in an ascending way. Then, the inverted image is cleaned to remove the noise in the image.

The fourth toggle mapping is based on the mean filter approximation. The noise criterion is top-hat checking at pixel point. If it is equal or less than a morphological transformation (opening and closing of white top-hat), it is left unchanged, otherwise, it is replaced with the multiplication of the mean value of opening and closing. Then, in order to filter noise in dark components, the inverted image is cleaned to remove the noise.

The fifth toggle mapping is based on gradient transformation. The noise criterion is an internal gradient which is the probability of the difference between the original image and dilation/erosion at the under-processed point. If it is equal or less than critical probability, it is left unchanged, otherwise, it is replaced with a multiplication of the mean value of opening/closing and closing/opening over 2 (α) [120]. In the case of white and dark component filtering, the noise criterion is changed in such a way that if the probability of the difference between the original image and dilation/erosion at pixel point is equal or less than a morphological transformation (opening and closing of the internal gradient), it is left unchanged, otherwise, it is replaced with α.

2.7 Transform domain-based filters

2.7.1 Framelet-based filters: These filters are processed in the domain which is not their original domain. There are some transformation domains such as frequency, wavelet [121–123], curvelet, and Framelet. The method in [124] proposed a frame-based [125] iterative algorithm for denoising. The methods such as AMF [39], ROAD [12], ACWMF [126] and MAD [127] are used as an initial step to detect/estimate the impulse noise. Then, a minimisation scheme is solved in order to remove the mixture of impulse and Gaussian noise as

$$\begin{aligned}\min\ F(c,\Omega) = \frac{1}{2}\| X_\Omega \bigcirc (\boldsymbol{D}c - y) \|_2^2 + \| \Lambda \bigcirc c \|_1 \\ + \frac{1}{2} \| (I - \boldsymbol{D}^{\mathrm{T}}\boldsymbol{D})c \|_2^2 + l_L(\Omega)\end{aligned} \tag{28}$$

where $L = [(1-p)d]$, $l_L(\Omega) = 0$ if $\| X_\Omega \| \le L$ otherwise $l_L(\Omega) = \infty$, Ω is the unknown observable region, X is the continuous function, y is the observed noisy image, Λ is the non-negative threshold value, d is the total number of pixels in the image, $\boldsymbol{D}$ is the tight frame, $\boldsymbol{D}^{\mathrm{T}}$ is the transpose of $\boldsymbol{D}$, p is the probability of impulse noise in the region Ω^c by Bernoulli trial and c is the frame coefficients of the image under a tight frame $\boldsymbol{D}$.

The frame-based iterative algorithm consists of two sub-problems which are solved iteratively and alternatively. In the first sub-problem, a frame-based convex minimisation with sparse and redundant directional representation is solved by using a balanced approach [128–130]. It is based on directional tensor product complex tight framelets [125, 131] which generates tight frames [128, 130]. It then restores the image in the transform domain by using these tight frames. In the second subproblem, the location of the impulse noise is estimated through l_0 minimisation. The results of this frame-based approach outperform those obtained with the method in [17], k-alternating least squares [132] and AOP [68].

2.7.2 Wavelet-based filters: The filter in [133] is based on a data-driven tight frame [134] which is a discrete compact wavelet frame. The tight frame uses the structural characteristics of the input image in order to perform image restoration. In the first step, a data-driven tight frame is used for a differential variation model as

$$\min_u \lambda_1 \| u - b \|_1 + \frac{\lambda_2}{2} \| u - b \|_2^2 + \rho \| W_u \|_1 \tag{29}$$

where λ_1, λ_2, and ρ are positive smoothing parameters, u is the original image, b is the noisy image, $\| \cdot \|$ is the fitting term and W_u is a tight wavelet frame in which $\| W_u \|_1$ is smoothing term. Here, the sparsity is used as a priori hypothesis of solutions. In the second step, the equation given earlier in (27) is solved using the augmented Lagrangian multiplier (ALM) method and the sub-problem is solved by the accelerated proximal gradient method [135]. The filter in [133] is shown to yield better performance than those filters in [135, 136].

2.7.3 DCT-based filters: The filter described in [137] is used for hyperspectral images. It assumes that each column of the image can be sparsely presented in the wavelet or DCT transform domains. This filter utilises the spatio-spectral correlation by expressing the image (X) as a sparse $Z = \boldsymbol{D}_1 X \boldsymbol{D}_2$ in which $\boldsymbol{D}_1$ is used for the spatial dimension (2D transform) and $\boldsymbol{D}_2$ is used for a spectral dimension (1D transform). The image can be defined as $\boldsymbol{D}_1^{\mathrm{T}} Z \boldsymbol{D}_2^{\mathrm{T}}$ because of the orthogonality of the DCT transform. Finally, the denoising problem can be expressed as a minimisation process as

$$\min_{Z,N_2} \| Z \|_1 + \| N_2 \|_1 + \lambda \| Y - \boldsymbol{D}_1^{\mathrm{T}} Z \boldsymbol{D}_2^{\mathrm{T}} - N_2 \|_F^2 \tag{30}$$

where λ is the regularisation parameter which is assumed to be 0.5, N_2 is the impulse noise, N_1 is the Gaussian noise defined as $Y - X - N_2$, with Y defining the noisy image. The expression $\| Y - \boldsymbol{D}_1^{\mathrm{T}} Z \boldsymbol{D}_2^{\mathrm{T}} - N_2 \|_F^2$ is minimised in order to reduce the effect of Gaussian noise. Then, the Split–Bregman method [138] is used for solving the equation defined earlier in (27). The filter in [137] is shown to have a better performance than the low-rank matrix recovery LRMR used in [139].

3 Comparison of methods

Table 1 provides the key points and limitations one ought to consider in the implementation of the numerous filters reviewed in this article. These limitations are based on empirical evaluations as reported in the literature and as implemented in this study.

For a comparative assessment, the most popular and prevalent methods are considered, and their performances are evaluated based on their implementation and the results they yield. Tables 2 and 3 compare the averaged peak signal to noise ratio (PSNR) and averaged image perceptual quality index [feature similarity index (FSIM)] [140] of some of the discussed mixed impulse and Gaussian denoising filters on 12 images commonly used in the literature on this particular research problem. The images of Lena, F16, Leaves, Boat, Couple, Fingerprint, Hill, Man, Peppers, Painting and Average are used for comparative purposes. Most of the methods listed in Tables 2 and 3 are based on statistical algorithms and their structural metrics are calculated on the average of the 12 testing images similar to those used in [83]. The comparison is done in the presence of impulse noise with 30%, 40%, and 50% noise intensity levels and Gaussian noise with the standard deviations of 0.1, 0.2, and 0.25. From the results provided in Tables 2 and 3, WESNR [83] shows in general a better performance among all other statistical algorithms studied.

Most of the methods in Tables 4 and 5 are based on the statistical methods (norm-based filters) and the PSNR and FSIM are calculated on the basis of 12 testing image (Lena, FG, Boat, Hill, Peppers, Man, Couple, AP, Cloth, Vase, Bush, and Flower) as in [96]. The comparison is done in presence of impulse noise with 10%–50% noise intensity levels and Gaussian noise with the standard deviations of 0.1–0.5. As tables show, low-rank

Table 1 Type of filters and current limitations

Type of filter	Limitations
spatial filters	averaging caused to blur the edges and consequently image
total variation filters	inappropriate estimation of the number of iteration caused to loss the details and over-smoothing
NLMs filters	complexity of weighting cause to computational burden
fuzzy-based filters	in the case of good mathematical descriptions and solutions, time and memory are two limitations for complete mathematical implementation
non-local similarity-based filters	detection of the best patches
	complexity cause to computational burden
	difficulty obeying quality constraints
maximum likelihood-based filters	difficulty obeying quality constraints
	sensitive to choose initial values
	it needs large samples to get optimal result
	the numerical estimation is non-trivial
	the mathematic is often non-trivial, particularly confidence intervals for the parameters is needed
sparsity-based filters	principled way to choose a solution for problem cause to computational burden and time consumption
	solving a noise-aware variant cause to sparse approximation and representation problem
inpainting-based filters	reproduction of large texture regions
	unable to recover partially degraded image
low rank approximation-based filters	complexity and high dimension of the matrix in order to solve the problem cause to computational burden. It could be a serious practical problem in the image
GP-based filters	very remarkable computing resources required
finite element-based filters	there is no general close-form solution (it can change in various parameters)
	the solutions are based on an approximation
	it has inherent errors which can cause to corrupt the image
morphological-based filters	it uses small images as structuring elements and acts as a moving probe that sample each pixel of image. It moves a fixed direction across the image, therefore, an artifact appears in the shape of structuring element
Framelet-based filters	their orientation selectivity is limited to only two directions
	complexity cause to computational burden
wavelet-based filters	scale and threshold selection are major problems, and avoiding blurring causes information loss

Table 2 PSNR comparison

		Type of denoising filter			
Gaussian noise (standard deviation)	Impulse noise (level), %	ROR-NLM [85]	Cai *et al.* [74]	$l_1 - l_0$ [73]	WESNR [83]
0.1	30	27.6027	29.8790	31.8109	31.3600
	40	26.5590	28.9290	30.6754	30.6309
	50	21.2990	27.8354	29.4290	29.6663
0.2	30	25.1118	27.6600	28.9027	31.4636
	40	24.1227	27.0627	28.1281	28.2509
	50	21.4790	25.4827	27.1900	27.4809
0.25	30	24.1327	26.7172	27.8636	27.9100
	40	23.0354	26.2172	27.1436	27.3154
	50	20.4409	25.4827	26.3172	26.5718

Table 3 FSIM comparison

		Type of denoising filter			
Gaussian noise (standard deviation)	Impulse noise (level), %	ROR-NLM [85]	Cai *et al.* [74]	$l_1 - l_0$ [73]	WESNR [83]
0.1	30	94.5000	95.6909	97.0154	96.7063
—	40	93.1700	94.5800	96.1927	96.1700
—	50	88.8263	89.5381	95.0400	95.3563
0.2	30	88.2336	92.3518	93.7163	93.6018
—	40	86.0090	91.2409	92.7163	92.8263
—	50	80.9609	89.5381	91.5227	91.7854
0.25	30	85.1118	90.5818	91.9881	92.2709
—	40	82.5336	89.5054	91.0718	91.2309
—	50	77.2509	87.8072	89.8200	90.1327

Table 4 PSNR comparison

Gaussian noise (standard deviation)	Impulse noise (level), %	Type of denoising filter						
		TPD [76]	BM3D [95]	WESNR [83]	SLR [98]	L_1-NLR [96]	L_0-NLR [96]	LSM-NLR [96]
0.1	10	28.78	30.57	30.24	30.50	31.25	31.36	32.30
	20	27.97	29.46	29.36	29.18	29.46	29.86	30.82
	30	27.15	28.30	28.40	27.82	27.74	28.55	29.37
	40	26.02	26.67	27.02	2620	26.74	26.92	27.24
	50	24.92	24.54	25.30	24.18	24.72	25.18	25.36
0.2	10	27.96	27.96	27.69	27.62	28.62	28.90	29.22
	20	25.84	27.21	27.09	26.79	27.50	27.78	28.27
	30	25.29	26.36	26.42	25.86	26.21	26.74	27.28
	40	24.37	24.97	25.24	24.54	24.83	25.37	26.08
	50	23.42	23.22	23.86	22.88	23.19	24.00	24.62
0.3	10	24.58	26.08	26.11	25.60	26.56	26.95	26.98
	20	24.21	25.39	25.55	24.85	25.49	25.92	26.20
	30	23.76	24.65	24.92	24.03	24.30	25.00	25.39
	40	22.95	23.35	23.74	22.83	23.11	23.74	24.33
	50	21.99	21.77	22.30	21.35	21.62	22.52	23.18
0.5	10	22.19	23.66	23.16	22.83	23.83	24.14	24.27
	20	21.94	22.99	22.59	22.18	22.73	23.20	23.61
	30	21.59	22.29	21.84	21.44	21.59	22.31	22.85
	40	20.87	21.05	20.78	20.35	20.73	21.14	21.95
	50	19.83	19.62	19.35	19.08	19.34	20.08	20.73

Table 5 PSNR comparison

Gaussian noise (standard deviation)	Impulse noise (level), %	Type of denoising filter						
		TPD [76]	BM3D [95]	WESNR [83]	SLR [98]	L_1-NLR [96]	L_0-NLR [96]	LSM-NLR [96]
0.1	10	95.59	97.11	96.65	97.11	97.48	97.57	97.63
	20	94.77	96.43	96.06	96.29	96.63	96.78	96.99
	30	93.78	95.43	95.25	95.15	95.32	95.78	96.17
	40	91.89	93.38	93.69	93.16	93.25	93.93	93.88
	50	89.60	89.58	90.99	89.63	90.23	90.96	91.00
0.2	10	93.76	93.76	92.82	93.66	94.29	94.77	94.78
	20	90.49	92.82	92.12	92.58	93.31	93.56	93.80
	30	89.43	91.52	91.27	91.18	91.91	92.15	92.67
	40	87.13	88.96	89.44	91.18	89.05	89.78	90.83
	50	84.70	85.19	87.07	88.73	85.86	86.70	87.92
0.3	10	86.98	90.11	90.19	85.14	91.06	91.67	91.68
	20	85.12	88.81	89.32	90.15	89.66	89.86	90.42
	30	84.92	87.33	88.30	88.73	87.91	87.96	89.17
	40	82.45	84.48	85.95	87.06	84.47	85.06	86.59
	50	79.89	80.73	82.93	84.32	81.13	81.93	83.78
0.5	10	79.84	84.04	82.71	80.72	85.19	85.54	86.31
	20	78.55	82.21	80.92	83.93	83.09	82.66	84.60
	30	77.31	80.51	78.94	82.02	80.82	79.86	82.72
	40	74.88	77.52	76.17	77.06	76.79	76.39	79.66
	50	72.37	74.04	72.51	73.71	73.53	73.74	76.80

approximation-based algorithm [96] has a better performance among other norm-based filters.

Fig. 2 shows a visual quality comparison of some state-of-the-art methods on the basis of one testing image, the Vase image as in [96], which is deemed sufficient for this type of comparison. As the results clearly indicate, LSM-NLR [96] has a better performance among all other denoising filters.

As reflected in the aforementioned Tables and Figures, statistical norm-based filters have yielded better performance among the filters that were implemented. In many algorithms, the characterisation of the complex distribution of mixed noise remains a major challenge. Some of them use conventional l-norms which don't perform well in the presence of mixed noise. WESNR [83] exploits the weighted encoding and sparse non-local regularisation to address such a challenge. Low-rank approximation-based filters have better performance than sparsity-based filters such as WESNR [83] and BM3D [95]. There is a problem in low-rank approximation-based filters in which they require a threshold selection in order to detect the Impulse noise. LSM-NLR filter [96] solved this problem by adaptively learning to define a threshold from the predicted noisy image and then use a non-local low-rank regularise (NLR) in order to complete the denoising process.

The PSNR measure is defined as:

$$\mathrm{PSNR} = 10\log\frac{(\max(I))^2}{\mathrm{MSE}} \tag{31}$$

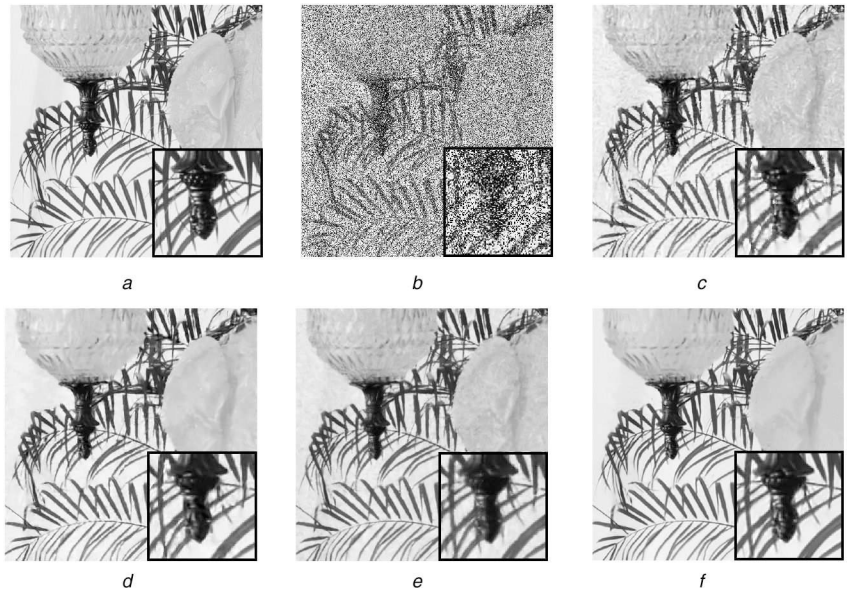

Fig. 2 *Denoising results of different filters on the test image 'vase' corrupted with Gaussian with standard deviation 20 and salt and pepper impulse noise with a 50% effect*

(a) Original image, ***(b)*** Noisy image, ***(c)*** Image denoised by BM3D [95], ***(d)*** Image denoised by WESNR [83], ***(e)*** Image denoised by SLR [98], ***(f)*** Image denoised by LSM-NLR [96]

where MSE is the mean square error as in (32) with max (x) defining the maximum pixel intensity of image I

$$\text{MSE} = \frac{\sum_{i=0}^{M-1}\sum_{j=0}^{N-1}(I(i,j)-D(i,j))^2}{M \times N} \tag{32}$$

Here I is the original image, D is the denoised image, M and N define the image's height and width. This measure is used to estimate the level of noise remaining in the denoised image. The FSIM [31] measures the degree of similarity and quality between the noisy original image and the denoised image. Equation (33) provides the formulation used for FSIM

$$\text{FSIM} = \frac{\sum_{i/\Omega} S_L(i) \,.\, \text{PC}_m(i)}{\sum_{i/\Omega} \text{PC}_m(i)} \tag{33}$$

where Ω is the whole image partial domain, $\text{PC}_m(i) = \max(\text{PC}_1(i), \text{PC}_2(i))$, PC maps extract from the noisy image and denoised image, $S_L(i)$ is the similarity at the location i. Note that in Tables 2–5, higher numbers are associated with better results.

4 Conclusion

Through this literature survey, we have presented the different classes of mixed impulse and Gaussian denoising filters and addressed the challenges involved in overcoming the combined effect of these two types of noise applied simultaneously on images. For comparative purposes, a randomly mixed noise model comprised of impulse (salt and pepper) and Gaussian noise is considered. An in-depth analysis of the noise models and denoising filters is presented. With this analysis, these noise models and denoising filters are classified according to their design types and domains of application. A comparative assessment is also provided in terms of their performance and the limitations they still experience. The broader implications of this research are outlined with two perspectives in mind: (i) discuss the design merits and application domains of these filters to help engineers and researchers solve related research problems in imaging, and be able to contend with the pervasive presence of noise, especially as it relates to the mixed effect of Gaussian and impulse noise and (ii) provide context on these denoising filters in terms of strengths and limitations of the type of filters considered in order to explore new avenues of research that could improve the performance of these filters. For these reasons, development of denoising algorithms must (i) reduce the blurring effects of smoothing, (ii) provide ideal selection of hyperparameters, (iii) perform accurate noise detection, (iv) optimise the denoising process, and (v) lessen the computational burden in the implementation process. Addressing these issues improves the prospects for a more realistic denoising process and makes such methods amenable to other domains of application.

5 Acknowledgments

We are grateful for the continued support from the National Science Foundation (NSF) under grants CNS-1920182, CNS-1532061, CNS- 2018611, CNS-1551221, CNS-1338922, and HRD-1834620. We also greatly appreciate the support of the FIU-University Graduate School (UGS) for the dissertation year fellowship provided to Mehdi Mafi.

6 References

[1] Prathiba, K., Rathi, R., Christopher, C.S.: 'Random valued impulse denoising using robust direction based detector'. Proc. IEEE Int. Conf. Information & Communication Technologies, Thuckalay, Tamil Nadu, India, 2013

[2] Healey, G.E., Kondepudy, R.: 'Radiometric CCD camera calibration and noise estimation', *IEEE Trans. Pattern Anal. Mach. Intell.*, 1994, **16**, (3), pp. 267–276

[3] Mafi, M., Martin, H., Adjouadi, M.: 'High impulse noise intensity removal in MRI images'. IEEE Signal Processing in Medicine and Biology Symp. (SPMB17), Philadelphia, PA, USA, 2017

[4] Mafi, M., Izquierdo, W., Adjouadi, M.: 'High impulse noise intensity removal in natural images using convolutional neural network'. Processing in 10th Annual Computing and Communication Workshop and Conf. (CCWC), Las Vegas, NV, USA, 2020

[5] Fareed, S.B.S., Khader, S.S.: 'Fast adaptive and selective mean filter for the removal of high-density salt and pepper noise', *IET Image Process.*., 2018, **12**, (8), pp. 1378–1387

[6] Li, F., Fan, J.: 'Salt and pepper noise removal by adaptive median filter and minimal surface inpainting'. Proc. IEEE 2th Int. Congress on Image and Signal Processing, Tianjin, China, 2009

[7] Liu, W., Lin, W.: 'Additive white Gaussian noise level estimation in SVD domain for images', *IEEE Trans. Image Process.*, 2013, **22**, (3), pp. 872–883

[8] Guo1, F., Zhang, C., Zhang, M: 'Edge-preserving image denoising', *IET Image Process.* ', 2018, **12**, (8), pp. 1394–1401

[9] Mafi, M., Martin, H., Andrian, J.*, et al.*: 'A comprehensive survey on impulse and Gaussian denoising filters for digital images', *Signal Process.*, 2019, **157**, pp. 236–260

[10] Buades, A., Coll, B., Morel, J. M.: 'A non-local algorithm for image denoising'. Proc. IEEE Int. Conf. on Computer Vision and Pattern Recognition, San Diego, CA, USA, 2005, **2**, pp. 60–65

[11] Coupe, P., Manjo, J. V., Robles, M.*, et al.*: 'Adaptive multiresolution non-local means filter for three-dimensional magnetic resonance image denoising', *IET Image Process.*., 2012, **6**, (5), pp. 558–568

[12] Garnett, R., Huegerich, T., Chui, C., *et al.*: 'A universal noise removal algorithm with an impulse detector', *IEEE Trans. Image Process.*, 2005, **14**, (11), pp. 1747–1754

[13] Tomasi, C., Manduchi, R.: 'Bilateral filtering for gray and color images'. Proc. IEEE Int. Conf. on Computer Vision, Bombay, India, January 1998

[14] Haijuan, H., Bing, L., Quansheng, L.: 'Removing mixture of Gaussian and impulse noise by patch-BasedWeighted means', *J. Sci. Comput.*, 2016, **67**, (1), pp. 103–129

[15] Bing, L., QuanSheng, L., JiaWei1, X., *et al.*: 'A new method for removing mixed noises', *Sci. China Inf. Sci.*, 2011, **54**, (1), pp. 51–59

[16] Donoho, D. L., Johnstone, J. M.: 'Ideal spatial adaptation by wavelet shrinkage', *Biometrika*, 1994, **81**, (3), pp. 425–455

[17] Delon, J., Desolneux, A.: 'A patch-based approach for removing impulse or mixed Gaussian-impulse noise', *SIAM J. Imaging Sci.*, 2013, **6**, (2), pp. 1140–1174

[18] Dong, Y., Chan, R., Xu, S.: 'A detection statistic for random-valued impulse noise', *IEEE Trans. Image Process.*, 2007, **16**, (4), pp. 1112–1120

[19] Jin, Q., Grama, I., Liu, Q.: 'Optimal weights mixed filter for removing mixture of Gaussian and impulse noises', *PLOS ONE*, 2017, **12**, p. 7, https://doi.org/10.1371/journal.pone.0179051

[20] Jin, Q., Grama, I., Kervrann, C., *et al.*: 'Non-local means and optimal weights for noise removal', *SIAM J. Imaging Sci.*, 2017, **10**, (4), pp. 1878–1920

[21] Jin, Q, Grama, I, Liu, Q.: 'A new Poisson noise filter based on weights optimization', *J. Sci. Comput.*, 2014, **58**, (3), pp. 548–573

[22] Delon, J., Desolneux, A., Guillemot, T.: 'PARIGI: a patch-based approach to remove impulse-Gaussian noise from images', *Image Process. Line*, 2016, **5**, pp. 130–154

[23] Hu, H, Li, B, Liu, Q.: 'Removing mixture of Gaussian and impulse noise by patch-based weighted means', *J. Sci. Comput.*, 2016, **67**, (1), pp. 103–129

[24] Smolka, B., Kusnik, D.: 'Robust local similarity filter for the reduction of mixed Gaussian and impulsive noise in color digital images', *Signal Image Video Process.*, 2015, **9**, (1), pp. 49–56

[25] Plataniotis, K., Androutsos, D., Venetsanopoulos, A.N.: 'Fuzzy adaptive filters for multichannel image processing', *Signal Process..*, 1996, **55**, (1), pp. 93–106

[26] Plataniotis, K., Androutsos, D., Venetsanopoulos, A.N.: 'Adaptive fuzzy systems for multichannel signal processing', *Proc. IEEE*, 1999, **87**, (9), pp. 1601–1622

[27] Plataniotis, K., Androutsos, D., Sri, V., *et al.*: 'Nearest-neighbour multichannel filter', *Electron. Lett.*, 1995, **31**, (22), pp. 1910–1911

[28] Plataniotis, K., Sri, V., Androutsos, D., *et al.*: 'An adaptive nearest neighbor multichannel filter', *IEEE Trans. Circuits Syst. Video Technol.*, 1996, **6**, (6), pp. 699–703

[29] Karakos, D., Trahanias, P.: 'Combining vector median and vector directional filters: the directional-distance filters'. Proc. Int. Conf. on Image Processing, Washington, DC, USA, 1995, **1**, pp. 171–174

[30] Viero, T., Oistamo, K., Neuvo, Y.: 'Three-dimensional medianrelated filters for color image sequence filtering', *IEEE Trans. Circuits Syst. Video Technol.*, 1994, **4**, (2), pp. 129–142

[31] Celebi, M.E., Kingravi, H.A., Aslandogan, Y.A.: 'Nonlinear vector filtering for impulsive noise removal from color images', *J. Electron. Imaging*, 2007, **16**, (3), paper number 033008

[32] Madhura, J., Ramesh Babu, D.R.: 'An effective hybrid filter for the removal of Gaussian-impulsive noise in computed tomography images'. Proc. IEEE Int. Conf. Advances in Computing, Communications and Informatics, Udupi, India, 2017

[33] Mafi, M., Rajaei, H., Cabrerizo, M., *et al.*: 'A robust edge detection approach in the presence high impulse noise intensity through switching adaptive median and fixed weighted mean filtering', *IEEE Trans. Image Process.*, 2018, **27**, (11), pp. 5475–5490

[34] Fabijan, A., Sankowski, D.: 'Noise adaptive switching median-based filter for impulse noise removal from extremely corrupted images', *IET Image Process..*, 2011, **5**, (5), pp. 472–480

[35] Su, T. J., Li, C. I.: 'An adaptive filtering method for mixed noise of images'. Proc. IEEE Int. Symp. on Computer, Consumer and Control, Taichung, Taiwan, 2012

[36] Huang, Y. M., Ng, M. K., Wen, Y. W.: 'Fast image restoration methods for impulse and Gaussian noises removal', *IEEE Signal Process. Lett.*, 2009, **16**, (6), pp. 457–460

[37] Hu, H., Li, F.: 'Image colourisation by non-local total variation method in the CB and YIQ colour spaces', *IET Image Process..*, 2018, **12**, (5), pp. 620–628

[38] Chambolle, A.: 'An algorithm for total variation minimization and applications', *J. Math. Image Vis.*, 2004, **20**, pp. 89–97

[39] Hwang, H., Haddad, R. A.: 'Adaptive median filters: new algorithms and results', *IEEE Trans. Image Process.*, 1995, **4**, (4), pp. 499–502

[40] Chen, T., Wu, H.: 'Space variant median filters for the restoration of impulse noise currupted images', *IEEE Trans. Circuits Syst. II, Analog Digital Signal Process.*, 2001, **48**, (8), pp. 784–789

[41] Eng, H., Ma, K.: 'Noise adaptive soft-switching median filter', *IEEE Trans. Image Process.*, 2001, **10**, pp. 242–251

[42] Pok, G., Liu, J., Nair, A.: 'Selective removal of impulse noise based on homogeneity level information', *IEEE Trans. Image Process.*, 2003, **12**, (1), pp. 85–92

[43] Rodríguez, P., Rojas, R., Wohlberg, B.: 'Mixed Gaussian-impulse noise image restoration via total variation'. Proc. IEEE Int. Conf. on Acoustics, Speech, and Signal Process, Kyoto, Japan, 2012

[44] Ko, S., Lee, Y.: 'Center weighted median filters and their applications to image enhancement', *IEEE Trans. Circuits Syst.*, 1991, **38**, (9), pp. 984–993

[45] Rudin, L., Osher, S. J., Fatemi, E.: 'Nonlinear total variation based noise removal algorithms', *Physica D. Nonlin. Phenomena*, 1992, **60**, (1–4), pp. 259–268

[46] Rodríguez, P., Wohlberg, B.: 'Efficient minimization method for a generalized total variation functional', *IEEE Trans. Image Process.*, 2009, **18**, (2), pp. 322–332

[47] Rodríguez, P., Wohlberg, B.: 'A generalized vectorvalued total variation algorithm'. Proc. IEEE Int. Conf. on Image Processing, Cairo, Egypt, 2009

[48] Langer, A.: 'Locally adaptive total variation for removing mixed Gaussian-impulse noise', *Int. J. Comput. Math.*, 2018, **96**, (2), pp. 1–23, doi: 10.1080/00207160.2018.1438603

[49] Hintermüller, M., Langer, A.: 'Subspace correction methods for a class of nonsmooth and nonadditive convex variational problemswithmixed L1/L2 data-fidelity in image processing', *SIAMJ. Imaging Sci.*, 2013, **6**, pp. 2134–2173

[50] Langer, A.: 'Automated parameter selection for total variation minimization in image restoration', *J. Math. Imaging Vis.*, 2017, **57**, pp. 239–268

[51] Chambolle, A., Pock, T.: 'A first-order primal–dual algorithm for convex problems with applications to imaging', *J. Math. Imaging Vis.*, 2011, **40**, pp. 120–145

[52] Agarwal, S.K., Kumar, P.: 'Denoising of A mixed noise color image using new filter technique'. Proc. IEEE Int. Conf. on Computational Intelligence and Communication Networks, Jabalpur, India, 2015

[53] Jain, A.K.: '*Fundamentals of digital image processing*' (Prentice-Hall, Upper Saddle River, NJ, USA, 1989, 1st edn)

[54] Gonzalez, R.C., Woods, R.E.: '*Digital image processing*' (Prentice-Hall, Upper Saddle River, NJ, USA, 2006, 3rd edn)

[55] Arnal, J., Sanchez, M.G., Vidal, V.: 'Parallel filter for mixed Gaussian-impulse noise removal'. Proc. IEEE Int. Conf. on Signal Processing: Algorithms, Architectures, Arrangements, and Applications, Poznan, Poland, 2013

[56] Morillas, S., Gregori, V., Hervás, A.: 'Fuzzy peer groups for reducing mixed Gaussian-impulse noise rom color images', *IEEE Trans. Image Process.*, 2009, **18**, (7), pp. 1452–1466

[57] Morillas, S., Gregori, V., Sapena, A.: 'Fuzzy bilateral filtering for color images'. Proc. Int. Conf. on Image Analysis and Recognition, Povoa de Varzim, Portugal, 2006, **4141**, pp. 138–145

[58] Kenney, C., Deng, Y., Manjunath, B. S., *et al.*: 'Peer group image enhancement', *IEEE Trans. Image Process.*, 2001, **10**, (2), pp. 326–334

[59] Astola, J., Haavisto, P., Neuvo, Y.: 'Vector median filters'. Proc. IEEE, 1990, **78**, (4), pp. 678–689

[60] Jayasree, M., Narayanan, N.K: 'A novel fuzzy filter for mixed impulse Gaussian noise from color images'. Int. Conf. on Signal, Networks, Computing, and Systems, New Delhi, India, 2016, pp. 53–59

[61] Passino, K., Yurkovich, S.: '*Fuzzy control*' (Addison Wesley, Menlo Park, CA, USA, 1998)

[62] Cox, E.: '*The fuzzy systems handbook*' (Academic, New York, USA, 1999, 2nd edn)

[63] Sun, Y., Junwei, H., Jun, L.: 'An information-fusion edge preserving method in image filtering'. Proc. IEEE Int. 16th Conf. on Wireless Communications Networking and Mobile Computing, Chengdu, China, September 2010

[64] Bing, Q., Xiaojun, J., Liangrui, T., *et al.*: 'Fingerprint image segmentation based on triangle module operator', *Comput. Eng.*, 2004, **30**, pp. 157–195

[65] Xuming, Z., Bingshi, C.: 'Adaptive median weighted mean hybrid filter', *Opt. Tech.*, 2004, **30**, (6), pp. 652–659

[66] Wang, J.H., Liu, W.J.: 'Histogram-based fuzzy filter for image restoration', *IEEE Trans. System, Man, Cybern, Part-B*, 2002, **32**, (2), pp. 230–238

[67] Pal, N.R., Pal, S.K.: 'Entropy: A new definition and its applications', *IEEE Trans. System, Man, Cybern, Part-B*, 1991, **21**, (5), pp. 1260–1270

[68] Guo, X., Guo, B.: 'A fuzzy filter for color images corrupted by mixed noise'. Proc. IEEE Int. Conf. on Identification, Information and Knowledge in the Internet of Things, Beijing, China, October 2014

[69] Lukac, R., Smolka, B., Plataniotis, K. N., *et al.*: 'Vector Sigma filters for noise detection and removal in color images', *Vis. Commun. Image R.*, 2006, **17**, pp. 1–26

[70] Chankhachon, S., Intajag, S.: 'Resourceful method to remove mixed Gaussian-impulse noise in color images'. Proc. IEEE 12th Int. Conf. on Computer Science and Software Engineering, Songkhla, Thailand, July 2015

[71] Camarena, J.G., Gregori, V., Morillas, S., *et al.*: 'A simple fuzzy method to remove mixed Gaussian-impulsive noise from color images', *IEEE Trans. Fuzzy Syst.*, 2013, **21**, (5), pp. 971–978

[72] Berg, M.D., Cheong, O., Kreveld, M.V., *et al.*: '*Computational geometry: algorithms and applications*' (Springer-Verlag TELOS, Santa Clara, CA, USA, 2008, 3rd edn)

[73] Xiao, Y., Zeng Yu, J., Ng, M.K.: 'Restoration of images corrupted by mixed Gaussian-impulse noise via 11–10 minimization', *Pattern Recognit..*, 2011, **44**, pp. 1708–1720

[74] Cai, J.F., Chan, R., Nikolova, M.: 'Fast two-phase image deblurring under impulse noise', *J. Math. Imaging Vis.*, 2010, **36**, pp. 46–53

[75] Elad, M., Aharon, M.: 'Image denoising via sparse and redundant representations over learned dictionaries', *IEEE Trans. Image Process.*, 2006, **15**, (12), pp. 3736–3745

[76] Cai, J., Chan, R.H., Nikolova, M.: 'Two-phase methods for deblurring images corrupted by impulse plus Gaussian noise', *Inverse Probl. Imaging*, 2008, **2**, pp. 187–204

[77] Wang, S.S., Wu, C.H.: 'New impulse detection and filtering method for removal of wide range impulse noises', *Pattern Recognit..*, 2009, **42**, pp. 2194–2202

[78] Nikolova, M.: 'A variational approach to remove outliers and impulse noise', *J. Math. Imaging Vis.*, 2004, **20**, pp. 99–120

[79] Filipović, M., Jukić, A.: 'Restoration of images corrupted by mixed Gaussian-impulse noise by iterative sost-hard thresholding', *Pattern Recognit..*, 2011, **44**, (8), pp. 1708–1720

[80] Mairal, J., Bach, F., Ponce, J., *et al.*: 'Online learning for matrix factorization and sparse coding', *J. Mach. Learn. Res.*, 2010, **11**, pp. 19–60

[81] Daubechies, I., Defrise, M., De Mol, C.: 'An iterative thresholding algorithm for linear inverse problems with a sparsity constraint', *Commun. Pure Appl. Math.*, 2004, **57**, (11), pp. 1413–1457

[82] Blumensath, T., Davies, M.E.: 'Iterative thresholding for sparse approximations', *J. Fourier Anal. Appl.*, 2008, **14**, (5–6), pp. 629–654

[83] Jiang, J., Zhang, L., Yang, J.: 'Mixed noise removal by weighted encoding with sparse nonlocal regularization', *IEEE Trans. Image Process..*, 2014, **23**, (6), pp. 2651–2662

[84] Dong, W., Zhang, L., Shi, G.*, et al.*: 'Image deblurring and superresolution by adaptive sparse domain selection and adaptive regularization', *IEEE Trans. Image Process.*, 2011, **20**, (7), pp. 1838–1857

[85] Xiong, B., Yin, Z.: 'A universal denoising framework with a new impulse detector and nonlocal means', *IEEE Trans. Image Process*, 2012, **21**, (4), pp. 1663–1675

[86] Dabov, K., Foi, A., Katkovnik, V.*, et al.*: 'Image denoising by sparse 3D transform-domain collaborative filtering', *IEEE Trans. Image Process.*, 2007, **16**, (8), pp. 2080–2095

[87] Yan, M.: 'Restoration of images corrupted by impulse noise and mixed Gaussian impulse noise using blind inpainting', *SIAM J. Imaging Sci.*, 2013, **6**, (3), pp. 1227–1245

[88] Jiang, J., Yang, J., Cui, Y.*, et al.*: 'Mixed noise removal by weighted low rank model', *Neurocomputing*, 2015, **151**, (part 2), pp. 817–826

[89] Ji, H., Liu, C., Shen, Z.*, et al.*: 'Robust video denoising using low rankmatrix completion'. Proc. IEEE 23th Int. Conf. on Computer Vision and Pattern Recognition, San Francisco, CA, USA, 2010

[90] Markosky, I.: '*Low rank approximation: algorithms, implementation, applications*', (Springer, London, 2012

[91] Liu, G., Lin, Z., Yu, Y.: 'Robust subspace segmentation by low-rank representation'. Proc. 27th Int. Conf. on Machine Learning, Haifa, Israel, 2010

[92] Liu, G., Lin, Z., Yan, S.*, et al.*: 'Robust recovery of subspace structures by low-rank representation', *IEEE Trans. Pattern Anal. Mach. Intell.*, 2009, **31**, (2), pp. 210–227

[93] Dong, W., Shi, G., Li, X.: 'Nonlocal image restoration with bilateral variance estimation: a low-rank approach', *IEEE Trans. Image Process.*, 2013, **22**, (2), pp. 700–711

[94] Zhang, L., Dong, W., Zhang, D.*, et al.*: 'Two-stage image denoising by principal component analysis with local pixel grouping', *Pattern Recognit..*, 2010, **43**, (4), pp. 1531–1549

[95] Dabov, K., Foi, A., Katkovnik, V.*, et al.*: 'Image denoising by sparse 3D transform-domain collaborative filtering', *IEEE Trans. Image Process.*, 2007, **16**, (8), pp. 2080–2095

[96] Huang, T., Dong, W., Xie, X.*, et al.*: 'Mixed noise removal via laplacian scale mixture modeling and nonlocal low-rank approximation', *IEEE Trans. Image Process.*, 2017, **26**, (7), pp. 3171–3186

[97] Dong, W., Shi, G., Li, X.*, et al.*: 'Compressive sensing via nonlocal low-rank regularization', *IEEE Trans. Image Process.*, 2014, **23**, (8), pp. 3618–3632

[98] Ji, H., Huang, S., Shen, Z.*, et al.*: 'Robust video restoration by joint sparse and low rank matrix approximation', *SIAM J. Imaging Sci.*, 2011, **4**, (4), pp. 1122–1142

[99] Dong, W., Zhang, L., Shi, G.*, et al.*: 'Nonlocally centralized sparse representation for image restoration', *IEEE Trans. Image Process.*, 2013, **22**, (4), pp. 1620–1630

[100] Eslahi, N., Mahdavinataj, H., Aghagolzadeh, A.: 'Mixed Gaussian-impulse noise removal from highly corrupted images via adaptive local and nonlocal statistical priors'. Proc. 9th IEEE Iranian Conf. on Machine Vision and Image Process, Tehran, Iran, 2015

[101] Candès, E., Demanet, L., Donoho, D.*, et al.*: 'Fast discrete curvelet transforms', *SIAM Multiscale Modeling Simul.*, 2006, **5**, (3), pp. 861–899

[102] Zhang, J., Zhao, D., Xiong, R.*, et al.*: 'Image restoration using joint statistical modeling in space-transform domain', *IEEE Trans. Circuits Syst. Video Technol.*, 2014, **24**, (6), pp. 915–928

[103] Goldstein, T., Osher, S.: 'The split Bregman method for `1 regularized problems', *SIAM J. Imaging Sci.*, 2009, **2**, (2), pp. 323–343

[104] Li, Y.R., Shen, L., Dai, D.Q.*, et al.*: 'Framelet algorithms for de-blurring images corrupted by impulse plus Gaussian noise', *IEEE Trans. Image Process.*, 2011, **20**, (7), pp. 1822–1837

[105] Khaw, H.Y., Soon, F.C., Chuah, J.H.*, et al.*: 'Image noise types recognition using convolutional neural network with principal components analysis', *IET Image Process..*, 2017, **11**, (12), pp. 1238–1245

[106] Aher, R.P., Jodhanle, K.C.: 'Removal of mixed impulse noise and Gaussian noise using genetic programming'. Proc. IEEE Int. Conf. on Signal Process, Beijing, China, October 2012

[107] Koza, J. R.: '*Genetic programming: on the programming of computers by means of natural selection*' (MIT Press, Cambridge, MA, USA, 1992)

[108] Banzhaf, W., Nordin, P., Keller, R. E.*, et al.*: '*Genetic programming: an Introduction—On the automatic evolution of computer programs and its applications*' (Morgan Kaufmann Publishers, San Mateo, CA, USA, 1998)

[109] Bishnu Lamichhane, P.: 'Finite element techniques for removing the mixture of Gaussian and impulsive noise', *IEEE Trans. Signal Process.*, 2009, **57**, (7), pp. 2538–2547

[110] Ciarlet, P.: '*The finite element method for elliptic problems*' (North-Holland, Amsterdam, The Netherlands, 1978)

[111] Brenner, S., Scott, L.: '*The mathematical theory of finite element methods*' (Springer–Verlag, New York, 1994)

[112] Quarteroni, A., Valli, A.: '*Numerical approximation of partial differential equations*' (Springer–Verlag, Berlin, Germany, 1994)

[113] Braess, D.: '*Finite elements: theory, fast solver, and applications in solid mechanics*' (Cambridge University Press, Cambridge, UK, 2001, 2nd edn)

[114] Civicioglu, P., Alci, M.: 'Impulsive noise suppression from highly distorted images with triangular interpolants', *AEU—Int. J. Electron. Commun.*, 2004, **58**, pp. 311–318

[115] Barber, C.B., Dobkin, D., Huhdanpaa, H.: 'The quickhull algorithm for convex hulls', *ACM Trans. Math. Softw.*, 1996, **22**, pp. 469–483

[116] Aurenhammer, F., Klein, R.: 'Voronoi diagrams', in Sack, J., Urrutia, J. (Eds) '*Handbook of computational geometry*' (North-Holland, Amsterdam, The Netherlands, 2000), pp. 201–290

[117] Mendiola-Santibañez, J. D., Terol-Villalobos, I. R.: 'Filtering of mixed Gaussian and impulsive noise using morphological contrast detectors', *IET Image Process..*, 2014, **8**, (3), pp. 131–141

[118] Beghdadi, A., Khellaf, A.: 'A noise-filtering method using a local information measure', *IEEE Trans. Image Process.*, 1997, **6**, (6), pp. 879–882

[119] Maragos, P., Schafer, R.: 'Morphological filters-part I: their set-theoretical analysis and relations to linear shift invariant filters', *IEEE Trans. Acoust. Speech Signal Process.*, 1987, **35**, pp. 1153–1169

[120] Richard, A. P.: 'A new algorithm for image noise reduction using mathematical morphology', *IEEE Trans. Image Process.*, 1995, **4**, (5), pp. 554–568

[121] Mafi, M., Tabarestani, S., Cabrerizo, M.*, et al.*: 'Denoising of ultrasound images affected by combined speckle and Gaussian noise', *IET Image Process..*, 2018, **12**, (12), pp. 2346–2351, doi: 10.1049/iet-ipr.2018.5292

[122] Li, X., He, M., Roux, M.: 'Multifocus image fusion based on redundant wavelet transform', *IET Image Process..*, 2010, **4**, (4), pp. 283–293

[123] Rabbouch, H., Saadaoui, F.: 'A wavelet-assisted subband denoising for tomographic image reconstruction', *J. Math. Imaging*, 2018, **55**, pp. 115–130

[124] Shen, Y., Han, B., Braverman, E.: 'Removal of mixed Gaussian and impulse noise using directional tensor product Complex tight framelets', *J. Math. Imaging*, 2016, **54**, (1), pp. 64–77

[125] Han, B.: 'Properties of discrete framelet transforms', *Math. Model. Nat. Phenom.*, 2013, **8**, pp. 18–47

[126] Chen, T., Wu, H. R.: 'Adaptive impulse detection using centerweighted median filters', *IEEE Signal Process. Lett.*, 2001, **8**, pp. 1–3

[127] Dong, Y., Chan, R. H., Xu, S.: 'A detection statistic for randomvalued impulse noise', *IEEE Trans. Image Process.*, 2007, **16**, pp. 1112–1120

[128] Cai, J. F., Chan, R. H., Shen, Z.: 'A framelet-based image inpainting algorithm', *Appl. Comput. Harmon. Anal.*, 2008, **24**, pp. 131–149

[129] Cai, J. F., Osher, S., Shen, Z.: 'Split bregman methods and frame based image restoration', *SIAM Multiscale Modeling Simulation*, 2009, **8**, pp. 337–369

[130] Shen, Y., Han, B., Braverman, E.: 'Image inpainting using directional tensor product complex tight framelets', arXiv:1407.3234v1, 2014

[131] Han, B., Zhao, Z.: 'Tensor product complex tight framelets with increasing directionality', *SIAM J. Imaging Sci.*, 2014, **7**, pp. 997–1034

[132] Wang, Y., Szlam, A., Lerman, G.: 'Robust locally linear analysis with applications to image denoising and blind inpainting', *SIAM J. Imaging Sci.*, 2013, **6**, pp. 526–562

[133] Ma, D., Wang, C.: 'Removal of mixed Gaussian and impulse noise using data-driven tight frames', *J. Eng. Sci. Technol. Rev.*, 2018, **11**, (2), pp. 26–31

[134] Cai, J.F., Ji, H., Shen, Z.*, et al.*: 'Data-driven tight frame construction and image denoising', *Appl. Comput. Harmon. Anal.*, 2013, **37**, (1), pp. 89–105

[135] Gong, Z., Shen, Z., Toh, K.C.: 'Image restoration with mixed or unknown noises', *SIAM J. Multiscale Modeling Simulation*, 2014, **12**, (2), pp. 458–487

[136] Yan, M.: 'Restoration of images corrupted by impulse noise and mixed Gaussian impulse noise using blind inpainting', *SIAM J. Imaging Sci.*, 2013, **6**, (3), pp. 1227–1245

[137] Aggarwal, H.K., Majumdar, A.: 'Mixed Gaussian and impulse denoising of hyperspectral images'. Proc. IEEE Int. Conf. Geoscience Remote Sensing Symp., Milan, Italy, 2015, pp. 429–432

[138] Goldstein, T., Osher, S.: 'The split bregman method for L1-regularized problems', *SIAM J. Imaging Sci.*, 2009, **2**, (2), pp. 323–343

[139] Zhang, H., He, W., Zhang, L.*, et al.*: 'Hyperspectral image restoration using low-rank matrix recovery', *IEEE Trans. Geosci. Remote Sensing*, 2014, **52**, (8), pp. 4729–4743

[140] Zhang, L., Zhang, L., Mou, X.*, et al.*: 'FSIM: A feature similarity index for image quality assessment', *IEEE Trans. Image Process.*, 2011, **20**, (8), pp. 2378–2386